

<https://doi.org/10.1038/s41540-025-00535-9>

Modeling the metabolic response of A2780 ovarian cancer cells to gold-based cytotoxic drugs

Walter Vieri^{1,4}, Veronica Ghini^{2,3}, Paola Turano^{2,3}, Lara Massai², Luigi Messori²✉ & Marco Fondi¹✉

Gold compounds are a promising class of experimental anticancer metallodrugs. Unlike platinum-based drugs, their antiproliferative effects are thought to result mainly from modulation of cancer cell metabolism rather than direct interaction with DNA. Previous NMR studies have shown that four cytotoxic gold compounds - auranofin, aurothiomalate and two gold N-heterocyclic carbenes - induce distinct metabolic changes in A2780 ovarian cancer cells, suggesting the occurrence of different mechanisms of action. To better understand these effects, we constructed a genome-scale metabolic model (GEM) of A2780 cells to analyze the NMR-detected metabolomic changes. The model successfully predicts the diverse metabolic responses induced by each gold compound and identifies common metabolic changes. These results confirm the potential of GEMs as a powerful tool for interpreting and predicting cellular responses to gold-based drugs, providing insights into their mechanisms of action and potential therapeutic applications.

Epithelial ovarian cancer (EOC) is the most common type of gynecological cancer in the Western world, with around 90 out of 100 ovarian tumors being epithelial. EOC means that the cancer started in the surface layer that covers the ovary¹. EOC is the eighth most common cause of cancer-related death in women, which can be explained by the late detection of the disease². Typically, tumors metabolize glucose by oxygen-independent aerobic glycolysis rather than the more efficient but oxygen-dependent process of oxidative phosphorylation, known as the Warburg effect³. This energetically disadvantageous process can be explained by the fact that the biosynthetic intermediates required for tumor proliferation are produced from glucose via pathways diverging from the central glycolytic cascade⁴. EOC exhibits a preference for using both aerobic glycolysis and mitochondrial oxidative phosphorylation to meet the energy demands of cancer cells and facilitate cell proliferation, invasion, and metastasis. The specific dominant pathway used by EOCs may vary depending on factors such as histological cell type, tumor aggressiveness, and tumor microenvironment⁵. Targeting and contrasting the preferred primary metabolism of EOC cells is a promising approach to combat chemoresistance. However, further research is needed to assess the clinical efficacy of these strategies in the treatment of EOC patients⁶.

The standard of care for EOC is primary debulking surgery followed by chemotherapy⁷. The most commonly used chemotherapy for EOC is platinum-based chemotherapy. Although promising, this therapy often

leaves patients with micro-metastases, which can eventually lead to disease recurrence, including the acquisition of platinum resistance. As platinum-based chemotherapeutics are not always effective, trials are needed to identify new therapies. New metal-based drugs have shown promising anticancer activity, and those based on gold appear to have a great potential, as gold tends to be less toxic to the human body than other metals such as platinum itself^{8–10}. Gold-based drugs deserve special attention because of the high electronegativity, electron affinity, and redox potential of the gold(I) center compared to the other metals¹¹. Gold compounds may contribute to cancer treatment through a variety of molecular mechanisms, including direct mitochondrial damage¹², alteration of DNA function¹³, and inhibition of thiol-containing enzymes¹⁴.

In the framework of a research program supported by the “Fondazione AIRC per la Ricerca sul Cancro”, IG 26169 - 2021 we have comparatively analyzed the “in vitro” anticancer activity of four different gold compounds and investigated their possible mode of action. The four gold(I) compounds considered here are auranofin (AF), aurothiomalate (AuTM), a gold N-heterocyclic monocarbene (AuNHC), and a gold N-heterocyclic dicarbene (Au(NHC)₂) complex. Notably AF and AuTM have been approved by FDA for the treatment of rheumatoid arthritis and are used here as repurposed drugs for cancer treatment¹⁰. AuNHC and Au(NHC)₂ are experimental anticancer drugs developed in our laboratory. The chemical structures of the four gold compounds are shown in Fig. 1. Based on

¹Department of Biology, University of Florence, Florence, Italy. ²Department of Chemistry, University of Florence, Florence, Italy. ³CERM, Florence, Italy. ⁴Present address: Department of Biology, University of Naples Federico II, Via Cinthia, 26 - 80126 Naples, Italy and Department of Agriculture, Food, Environment and Forestry (DAGRI), University of Florence, Florence, Italy. ✉e-mail: luigi.messori@unifi.it; marco.fondi@unifi.it

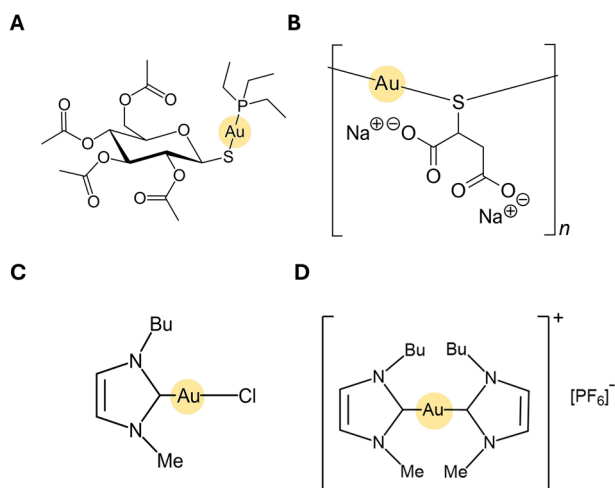


Fig. 1 | The chemical structure of the four gold compounds. A AF; B AuTM; C AuNHC; D Au(NHC)₂.

previous studies, these gold compounds are known to have very relevant and promising antiproliferative properties^{15–18}.

While studying their biological and cellular effects, we realized that these gold compounds can induce important changes in the metabolism of cancer cells, which may be the basis of their remarkable anti-proliferative effect. Mechanistic studies of these compounds are typically based on omics approaches^{19–22}. Complete sets of comparative NMR metabolomics data have been collected for these four gold compounds, as described in more detail below. As the patterns of observed changes in the cellular metabolome are highly variable, we have attempted to interpret this complex situation in terms of the likely molecular mechanisms and key biological processes affected by each compound, and to correlate the chemical structure of these gold compounds with their respective pharmacological profiles.

Genome-scale metabolic models (GEMs) allow the analysis, the simulation and the prediction of the cellular responses activated under different conditions. This helps to understand the cellular functions, metabolic pathways, and impact of genetic and environmental factors on the overall metabolic rates of these processes²³. Constraining GEMs with omics data allows the creation of specific tissue models and can improve their predictive ability. Creating a context-specific human model from Recon3D, for example, has suggested new drug targets with greater accuracy and has led to the development of novel targeted therapies for any disease^{24,25}.

Here, we reconstructed a tissue-specific model of EOC from A2780 into the most widely used human GEM model, Recon3D. We further constrained the model with NMR metabolomics data measured in the 4 different gold-based drug treatments and associated controls. For each treatment, we were able to simulate fluxes in the metabolic network using Flux Balance Analysis (FBA) and Flux Sampling (FS) to identify drug-targeted pathways, common patterns, and drug-specific patterns.

Results

Comparative analysis of NMR metabolomics data of gold drugs in A2780 cancer cells

NMR metabolomics is a powerful tool for monitoring changes in the cellular metabolome induced by drug treatment²⁶. The method has the potential to identify and quantify the main endo- and exo-metabolites of cancer cells in a very reproducible manner. Analysis of the observed changes can provide a detailed insight into the specific actions of a given drug, its effects on the different compartments of cellular metabolism, its possible mode of action and the cellular response to damage. Recently, we used this method to analyze the changes in the metabolome of A2780 cancer cells induced by the four cytotoxic gold compounds mentioned above, using A2780 cancer cells as a reference model²¹. The results were first published in three separate

papers^{18,27,28}. The first paper analyzed the effects of auranofin; the second paper compared the metabolic changes induced by the monocarbene and dicarbene gold complexes. The third paper compared the metabolic changes induced by aurothiomalate (and its ferritin adduct under equitoxic conditions). The results of these studies are summarized in Figs. 2, 3. Figure 2 shows the ¹H NMR spectra of cell lysates (A–B) and growth media (C–D) for A2780 cells with AuNHC, Au(NHC)₂, AuTM and AF for 24 h. Figure 3 reports synoptically observed quantitative changes. Endo- and exo-metabolites detected by NMR are shown together with the significant changes in their concentration observed upon treatment with the four different cytotoxic gold drugs. The changes are measured after 24 h of treatment using a concentration of the Au(I) drugs equal to their respective IC₅₀ values at 72 h (in such a way to work under equitoxic conditions); based on previous time course studies, 24 h represents the shortest time where we could observe significant effects for all compounds^{18,27,28}.

A few general conclusions can be drawn from inspection of these data:

1. Overall, the four gold compounds have an important effect on the metabolism of A2780 cancer cells, supporting the view that these changes in metabolism may play a critical role in the respective mechanisms of cytotoxicity. More in detail, we found that AF induced significant changes to 22 metabolites (11 extracellular and 11 intracellular), AuNHC to 22 (14 extracellular and 8 intracellular), Au(NHC)₂ to 35 (22 extracellular and 13 intracellular) and AuTM to 13 (9 extracellular and 4 intracellular).

2. While some common features of the four gold compounds could be identified (such as an increased secretion of lactic acid, although not significant for AuTM, see Fig. 3B, and a greatly reduced secretion of pyruvate), the metabolic changes induced by the four gold compounds appear to be quite different from one another, suggesting that the four gold compounds have substantially different modes of action. However, there are some apparent similarities in the profiles of AuNHC and Au(NHC)₂ that deserve attention.

3. The specificity of the metabolic responses induced by each gold compound can be summarized as follows:

i) Auranofin induces a large increase in glutathione and only a small increase in lactate.

ii) The two gold carbenes cause an increase in glycolysis and induce the production of a very large amount of lactate, with no significant increase in GSH (it even decreases upon Au(NHC)₂ treatment).

iii) Aurothiomalate produces relevant changes in the TCA metabolites, but no increase in lactate; an increase in GSH (significant after 48 h, data not shown) is observed, although less than in the case of AF.

While this survey of previously collected data revealed interesting correlations between these gold drugs and their effects on cellular metabolism, it also showed only the end point(s) of such effect(s). In fact, the change in concentration of a given intracellular metabolite may be due to the action of several (possibly conflicting and/or interacting) pathways, the contribution of which cannot be deduced from the concentration of the end-product alone. Therefore, to characterize the effect of each tested compound on the overall cellular metabolism and to identify the pathways most likely to be affected by the action of the different drugs, we used genome-scale modeling of ovarian cancer cells, as described in the next sections.

Context-specific genome-scale reconstruction

To investigate the impact of the four different gold-based compounds on the potential system-level functional metabolic shifts in the A2780 ovarian cancer cell line, we reconstructed context-specific genome-scale metabolic models. The procedure we used is detailed in Materials and Methods and schematically shown in Fig. 4A. Briefly, the construction of this model started with the latest global human metabolic reconstruction called Recon 3D. We used the gene expression data of the A2780 cell line from the Cancer Cell Line Encyclopedia²⁹ and the GIMME algorithm³⁰ to constrain it.

This involved matching the gene identifiers in the RNA-seq dataset to those in the RECON3D reconstruction. All genes were correctly mapped, except for 30 for which we could not automatically find a match. After manually curating genes of this subset, we were left with 3 unidentified genes

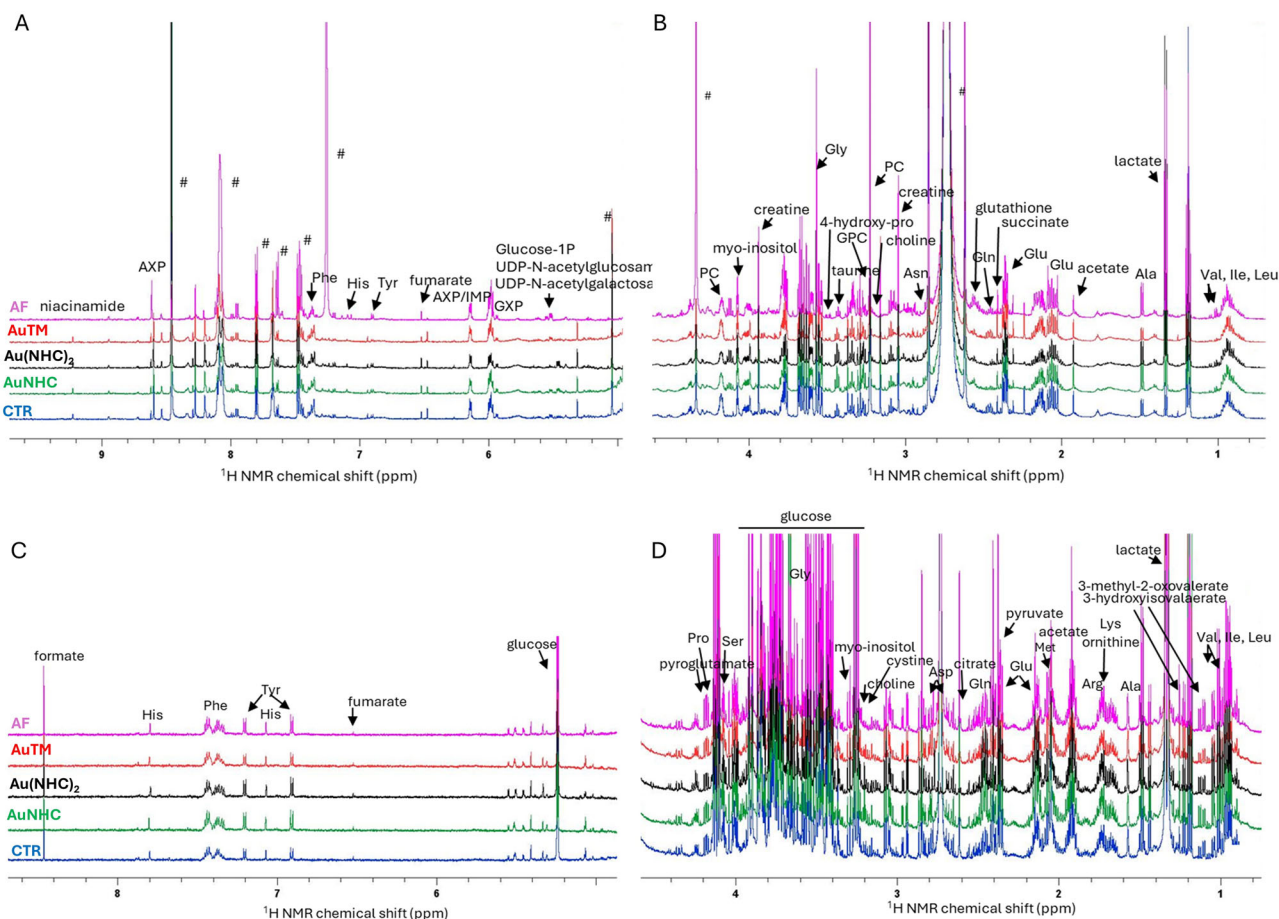


Fig. 2 | Representative ^1H NMR spectra of A2780 control cells and A2780 cells treated with AuNHC, Au(NHC) $_2$, AuTM and AF for 24 h. Cell Lysates (A, B) and growth media (C, D). #: signals of the protease and phosphatase inhibitor cocktail.

in the NCBI Entrez gene list and decided to set their expression level in the model to the maximum observed TPM value (see below), as done in Weglarz-Tomczak et al.³¹. This guarantees that they will not be limiting in any of our downstream analyses. Next, it was necessary to define an expression threshold to consider a gene (i.e. an enzyme) active in the context-specific metabolic reconstruction, given the A2780 expression values. As there is no generally accepted threshold in this sense, we used an “elbow strategy” to define the most reasonable gene expression threshold. Specifically, we used the “elbow” cut-off point (as is usually done in heuristic mathematical optimizations) to select the expression values for which adding additional genes to the model didn’t significantly affect the outcome of the main model features (i.e. number of metabolites, reactions and cancer-associated reactions).

The results of this analysis are shown in Fig. 4B. We found that a gene expression threshold of 0.5 TPM shrank the original (i.e. TPM threshold equal to 0) unconstrained metabolic model (as expected), but retained most model features and, perhaps more importantly, these features were not affected by further changes in the expression threshold. After some manual curation, such as adding back 23 transport reactions for metabolites known to be consumed by cells during in vitro growth, the final model contained 3769 metabolites and 4930 reactions. While the latter represented less than 50% of the reactions present in the original human reconstruction (Recon3D), the initial unconstrained optimal solution was very similar between the two models, suggesting that no important pathways were removed during the creation of the ovarian cancer-specific metabolic model. Furthermore, in the A2780 GEM, we retained 79 of the 116 total cancer-related responses found in the literature (Table S1)^{32–35}. We then sought to further contextualize the A2780 GEM and investigate its metabolic response to gold-based compounds.

To do this, we constrained the nutrient uptake responses according to the experimental data on the relative concentration of metabolites measured in the medium at time 0 and 24 h. In total, we obtained 46 context-specific GEMs each, which we used for downstream simulations. These were 16 models reproducing the exposure to auranofin (8 control and 8 treated samples), 12 to aurothiomalate (6 control and 6 treated samples), 12 to gold monocarbene (6 control and 6 treated samples) and 6 to gold dicarbene (6 treated samples) at $t = 24$ h and the respective control at $t = 0$ h. Note that the 6 gold monocarbene controls are shared with gold dicarbene (3) and with aurothiomalate control pools (3). We would like to point out that to constrain the models, we only used metabolomic data from the growth media (Fig. 3B). In this way, we were able to use intracellular metabolomic data (cell lysate, Fig. 3A) as a benchmark and validate whether the contextualized model could be used to correctly represent the intracellular metabolic state of the cells. Furthermore, the contextualization of metabolic reconstructions with intracellular metabolite concentrations could lead to ambiguous results. Indeed, for a single measured compound, there are usually multiple reactions (i.e. enzymes) responsible for its production/consumption and identifying which of these is responsible for the observed change could be misleading in the absence of additional information.

Overall metabolic reprogramming induced by gold compounds

First, Flux Balance Analysis (FBA) was employed to optimize the biomass objective function. Subsequently, flux sampling (FS) was utilized to analyze the probability distribution of reaction fluxes within the metabolic network, to investigate metabolic reprogramming because of gold-based drug exposure from a general perspective (Fig. S1A–H). When simulating auranofin exposure, 107 reactions showed a significant change in their activity when comparing the A2780 model with the auranofin-specific A2780

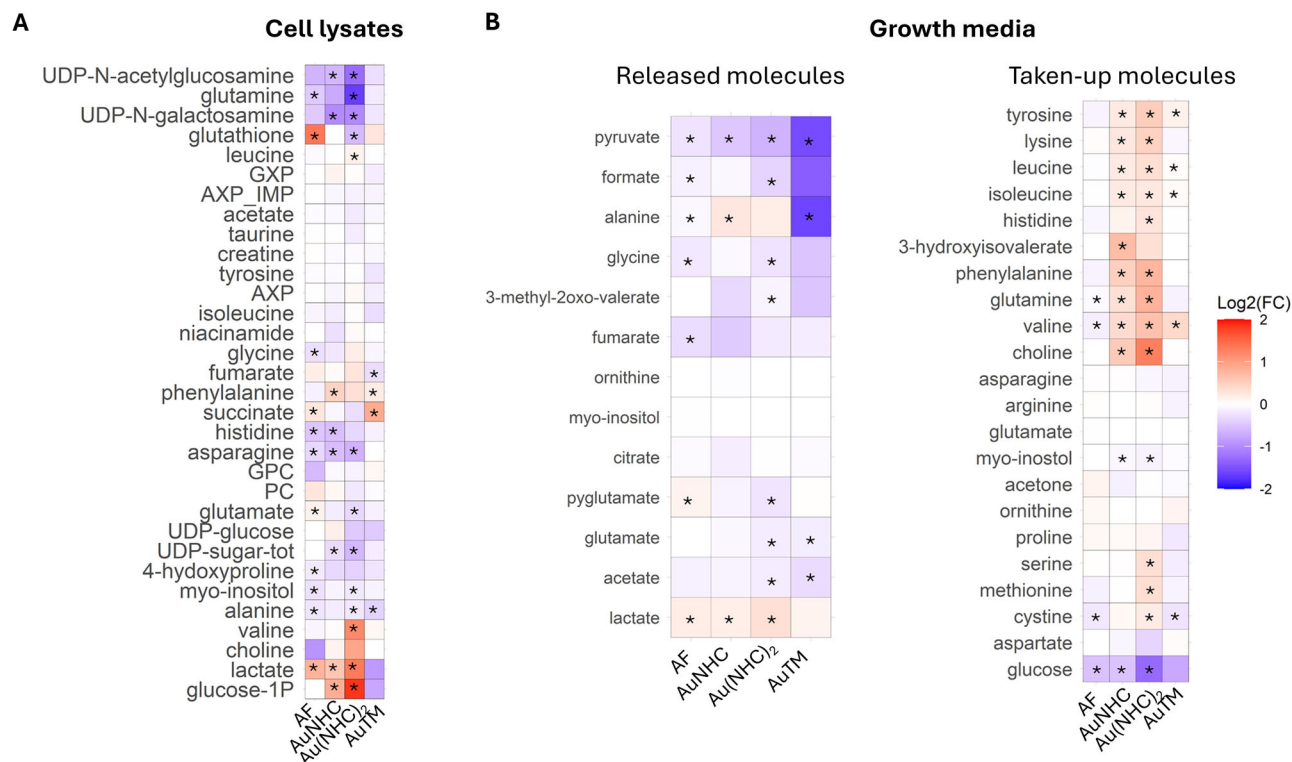


Fig. 3 | Level plot of fold changes upon 24 h of treatment of A2780 cells with AF, AuNHC, Au(NHC)₂ and AuTM. A Intracellular metabolites (cell lysates) and **B** extracellular metabolites (growth media). Red/blue colors indicate the higher/lower metabolite concentration in Au(I) drug-treated cells with respect to control samples (Log₂(FC)). In panel (B), the metabolites are divided into two different classes, i.e. those that are taken up from the medium and those that are released into the medium. To be noted that the FC refer to the relative concentration of each

metabolite in the samples; thus, for the molecules that are released, lower/higher concentration levels upon treatment mean a lower/higher release; Indeed, for the molecules that are taken up from the starting media, lower/higher levels upon treatment mean a greater/lower consumption of nutrients, i.e. increased/decreased uptake. The brightness of the colors corresponds to the magnitude of FC. Asterisks indicate statistical significance (p value < 0.05).

model (Fig. S1A–H). Of these, 62 increased or decreased their flux in the treated condition, while 45 changed their direction.

Interestingly, among the reactions that increased their activity upon auranofin exposure, we found the reaction SSALxm (succinate-semialdehyde:NAD⁺ oxidoreductase), which is responsible for an increase in mitochondrial succinate. Of note is the reaction involving the thioredoxin RNTR1, which shows an increase in negative flux and reduced thioredoxin production. Theoretically, thiol-redox enzymes such as thioredoxin reductase (TrxR) and thioredoxin glutathione reductase (TGR) are inhibited by auranofin³⁶. Among the 45 significant reverse reactions, many involve transport (HMR_2706, HMR_2857) and carnitine production with coenzyme A consumption. Finally, three reactions are significant in both FS and FBA: FUMtr, increasing extracellular fumarate; EX_fum_e, decreasing fumarate secretion; and MALSO3tm, increasing malate transported from the mitochondria to the cytosol, thus diverting it from the Krebs cycle.

For aurothiomalate we observed 126 reactions with significantly different flux values, 99 with the same direction and 27 with the opposite direction (Fig. S1B). Several significant reactions involve fatty acids, particularly with a decrease in flux in reactions FACOAE1839Z12Z15Z and FACOAL1832, resulting in reduced coenzyme A consumption and less alpha-linolenoyl-CoA production. The FACOAL161 reaction consumes more coenzyme A and produces hexadecenoyl-CoA, a precursor in the essential carnitine synthesis pathway of lipid metabolism. Carnitine is key in facilitating the transport of long chain fatty acids into the mitochondria for β -oxidation. Two reactions with a significant increase in flux leading to carnitine production are LNELDCCPT1 and LNELDCCPT2. Five reactions are involved in the metabolism of long-chain fatty acid β -oxidation: FAOXC160, FAOXC10080m, FAOXC142C122m, FAOXC183C163Gm and FAOXC18480x, leading to reprogramming of this pathway. Fatty acid

metabolism plays a central role in cancer, serving not only as structural components of membranes, but also as important secondary messengers and potential fuel sources for energy production^{37,38}. We observed an increased consumption of galactose in the following reactions: GALKr in the cytosol, and GALASE10ly, GALASE11ly, and GALASE12ly in the lysosome. Other significant reactions include PEPCKm with increased oxaloacetate consumption and phosphoenolpyruvate production, and GTHS with higher reduced glutathione production.

In the pool of 151 reactions significantly affected by AuNHC exposure (Fig. S1C), we found twelve reactions that involve long-chain fatty acid β -oxidation, and four isomerization reactions of fatty acids all of which show significantly reduced flux in the treated model compared to the control (FAOXC2452256x, FAOXC164C165m, FAOXC164C143m, FAOXC164m, FAOXC165C164m, FAOXC103C102m, FAOXC102C103m, FAOXC102m, FAOXC143C123m, FAOXC123m, FAOXC102C81m, FAOXC81C61m, FAOXC123C102m, FOX61, FAOXC225C226x, FAOXC226C225x). As said, this metabolic process is pivotal in cancer development. Another cluster of significant reactions involves N-acetylglucosamine 6-O-sulfotransferase in the lysosome and Golgi (S6TASE10ly, S6TASE16ly, S6TASE20ly, S6T1g, S6T2g, S6T3g, S6TASE17ly, S6TASE21ly), with a general 32% reduction in flux in these reactions in the treated model. N-Acetylglucosamine 6-O-sulfotransferase-2 is expressed in mucinous carcinomas and ovarian cells³⁹ and a decrease in the flux of some reactions involved in this pathway may indicate another pathway affected by the drug. Finally, several reactions involved in beta-galactosidase, all of which reverse their flux compared to the treated model, consume D-galactose in the lysosome (GALASE9ly, GALASE8ly, GALASE7ly, GALASE6ly, GALASE5ly, GALASE4ly, GALASE3ly).

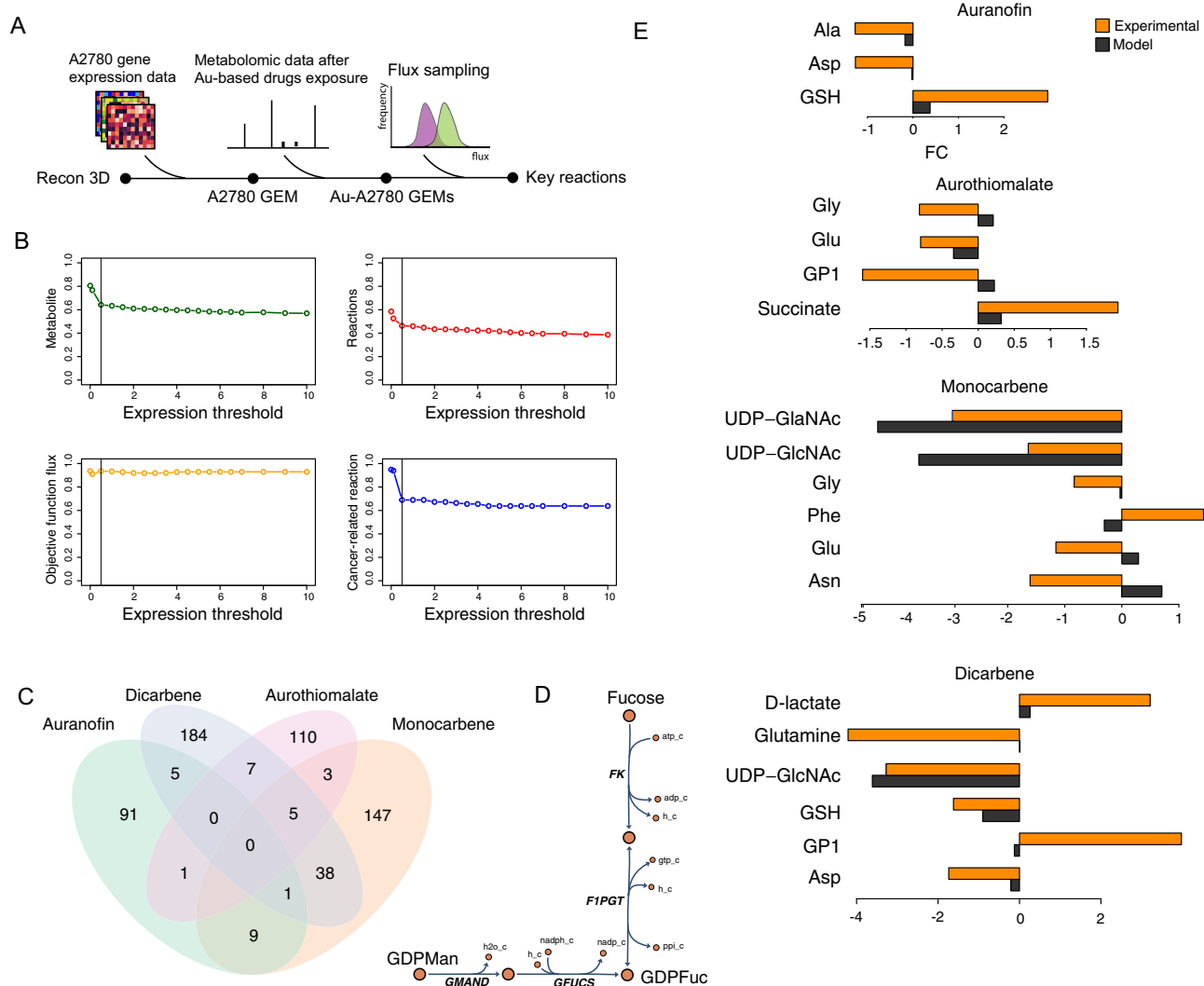


Fig. 4 | Overview of A2780 GEM reconstruction and modeling. A Scheme of the genome-scale metabolic reconstruction of A2780 cells. **B** Expression level threshold adopted here and its impact on metabolites, reactions, cancer-related reactions and biomass reaction flux. **C** Venn diagram showing the pool of shared reactions

between the four context-specific models. **D** Schematic representation of the main metabolic nodes around the compound Fucose. **E** Comparison between measured and simulated changes in specific metabolites for each treatment.

Like AuNHC and aurothiomalate, Au(NHC)₂ has numerous significant reactions related to fatty acid beta-oxidation, resulting in an overall reduction in acetyl-CoA production (Fig. S1D). Two reactions with the highest fold change between control and treatment involve lysosomal N-acetylglucosamine 6-O-sulfotransferase, like monocarbene, with an inverted flux. Among the significant reactions, there is a significant flux reduction in the ACONT reaction, leading to the formation of isocitrate from citrate. Notably, mutations in isocitrate dehydrogenase (IDH) downstream of ACONT contribute to tumorigenesis. Therefore, reduced isocitrate production may contribute to reduced activity in the reactions in which it is involved^{40,41}.

This dataset of reactions that appear to be stimulated by exposure to the different gold-based compounds allows us to test whether the four gold-based compounds elicit a common response at the level of the whole metabolism (Fig. 4C). As expected, we found that the lactate exchange reaction is shared by contextualized monocarbene, dicarbene and auranofin models, an observation that reflects the limitation of models based on extracellular metabolite concentration (Fig. 4B).

Five reactions are shared by aurothiomalate and the two gold N-heterocyclic carbene. Apart from pyruvate exchange (which shows a reduced positive flux in all three drug-treated conditions, hence less

secretion, Fig. 4D), the remaining four reactions revolved around the metabolism of GDP-L-fucose (reactions FK, F1PGT and GFUCS and GMAND, Fig. 4D), showing a general reduction in fluxes. Although without statistical support, the same trend was observed in the analysis of auranofin context-specific models (data not shown). Thus, according to our simulations, the reduction of intracellular fluxes around the GDP-L-fucose node could represent a general response of A2780 cells to gold-based treatment. It is interesting to note that cancer progression has been shown to be associated with increased GDP-fucose production, which may support tumor cell proliferation and survival⁴². The availability of the high-energy donor GDP-fucose can lead to aberrant fucosylation, i.e. the process of transferring fucose from GDP-fucose to its substrates, a mechanism that has been shown to play a relevant role in many aspects of cancer biology⁴³.

Flux sampling on context-specific GEMs and comparison with measured metabolites

Next, we used FS to investigate the metabolic reprogramming induced by exposure to gold-based compounds in A2780 cells. First, we compared the predictions of context-specific models with the measured intracellular levels of metabolites. We limited this comparison to those metabolites whose change in intracellular concentration was significant when comparing

treated and untreated samples. As shown in Fig. 4E, we found that the context-specific model predictions agreed with the experimental data in about 70% of the cases (13 out of 19). For each of the four treatments, we then searched the context-specific models for reactions with a significant change in flux in the treated vs. untreated comparison that could reveal the hidden metabolic consequences of gold drug-exposed cells.

Auranofin. The FS data for auranofin suggested an overall increase in glutathione production and a decrease in arginine and alanine production, trends consistent with the measured levels of these metabolites (Fig. 3E). For this increase in GSH production, the model suggests an alternative pathway involving the utilisation of aminobutyric acid instead of cysteine⁴². Our simulations identify reactions involving the production of aminobutyric acid, specifically ABTA_{rm}, as increasing its flux. This reaction results in the production of aminobutyric acid along with 2-oxoglutarate while consuming glutamate. Instead, cysteine is mainly consumed by the PPNCL2 reaction. With regard to asparagine, the major reaction involving this metabolite is r1630, which is responsible for its transport out of the cytosol, leading to a decrease in its intracellular concentration. Cytosolic asparagine is essential for protein synthesis and some studies suggest that intracellular asparagine is a critical suppressor of apoptosis in many human tumors^{44,45}.

For alanine, we observed a general decrease in the flux distributions of reactions using it as a substrate, although none of the distributions were statistically significant from the controls. Concerning GHS metabolism, in a recent paper, Chiappetta et al. showed the up-regulation of the NRF2-controlled proteins GCLC and GCLM in AF-treated cells²². Notably, these proteins are involved in GHS biosynthesis and the AF context-specific model predicted an increased flux through the corresponding reactions compared to the control model.

Aurothiomalate. Regarding aurothiomalate, the significant metabolites in the experiments, also present in the model, showed the same trend of fold change in two cases: glutamate (decrease) and succinate (increase) (Fig. 3E). For succinate, there is a general increase without a specific response, providing insight into a metabolic pathway that specifically contributes to its increase. For glutamate, however, we found a significant change in the flux of the reaction PSERT (phosphoserine transaminase), which leads to glutamate consumption and 2-oxoglutarate production with a flux four times higher than the control. Interestingly, this reaction could also explain the change in succinate concentration, as 2-oxoglutarate can feed the TCA cycle, leading to an increase in its production.

AuNHC. In the context of gold N-heterocyclic monocarbene treatment, three metabolites show consistent flux direction with experiments, namely glycine (decrease), UDP-N-acetylglucosamine (UDP-GlcNAc) (decrease) and UDP-N-acetylgalactosamine (UDP-GalNAc) (decrease, Fig. 3E). According to our model, glycine is mainly consumed via the GTHS reaction (glutathione synthetase), resulting in reduced glutathione production in the cytosol. The activity of this reaction is supported by the transport of glycine in the cytoplasm by the reaction GLYSNAT5tc: in contrast to the control models, in the model resembling the monocarbene treatment, this reaction shows a significant import flux, thus potentially favoring the activity of the GTHS reaction. Conversely, the THRGLYexR reaction (threonine-glycine exchange reaction) facilitates the export of glycine from the cytosol and the import of threonine, although with a reduced flux compared to the former reaction.

For UDP-GlcNAc, ten significant reactions are likely to induce a major reprogramming of its pathway. Four reactions contribute to the overall reduction of UDP-GlcNAc: two are associated with increased metabolite consumption with UDP, GALNACT2g and HMR_7180 production, while two show reduced production compared to the control (AG13T2g and AG13T1g). The R0845 reaction is active in the treated model and mediates UDP-GlcNAc transport. In addition, the AG13T17g reaction consumes

UDP-GlcNAc in the control but shows no flux in the treated model, GALNACT5g consumes less in the treated model, AG13T16g, inactive in the treated model, consumes UDP-GlcNAc in the control and GALGT1 CORE2GTg is responsible for its production. Interestingly, the HMR_7180 reaction consumes not only UDP-GlcNAc but also the Tn antigen, which is associated with disease progression many tumor⁴⁶. The third significant metabolite in the experiments that shows a congruent trend in our flux data is UDP-GalNAc; in this case, no significant reactions contribute to its reduction, but two significant reactions lead to its production: GALGT1 and GALNACT1g. Another reaction, UGALNACTg, reduces transport from the cytosol to the Golgi. However, the decrease in UDP-GlcNAc upstream in the pathway leading to UDP-GalNAc production may explain its overall decrease in the treated model⁴⁷.

Au(NHC)₂. Metabolites that show significant changes in the experimental data with consistent flux patterns include alanine (decrease), asparagine (decrease), glutathione (decrease), phenylalanine (increase), UDP-N-acetylglucosamine (UDP-GlcNAc) (decrease), UDP-N-acetylgalactosamine (UDP-GalNAc) (decrease) and D-lactate (increase) upon dicarbene treatment (Fig. 4C and Supplementary Fig. S1D). Alanine is affected by significant transport-related reactions to and from the cytosol: ALAGLYexR, r1701, r1918 and r1883 show a reduced flux compared to the control, indicating reduced extracellular transport. However, reaction r1563 shows an inverted flux and an increased transport out of the cytosol. The change in asparagine concentration is mostly related to transport-related reactions, such as ASPNHEAT2tc, with an inverted flux and increased transport outside the cytosol, whereas r1837 and r1757 show a significant decrease in flux in the opposite direction. Phenylalanine shares a transport reaction with asparagine, ASPNHELAT2tc, which increases its transport into the cytosol.

The model reflects an increase in lactate through a single significant reaction (EX_lac_L_e), indicating increased extracellular transport. UDP-GlcNAc decreases, in agreement with experimental data, mainly in the GALNACT2g reaction, with an inverse flux leading to UDP-GlcNAc consumption. However, other reactions contribute to increased UDP-GlcNAc production, such as AG13T18g, or decreased consumption compared to the control, such as AG13T16g and UAG4Ei, the latter resulting in reduced production of UDP-GalNAc, another important metabolite. No significant GHS-related responses were observed.

Discussion

NMR metabolomics studies previously performed in our laboratory on A2780 ovarian cancer cells showed that the patterns of changes induced by four representative cytotoxic gold compounds, i.e. auranofin, aurothiomalate, and the two gold-N-heterocyclic carbenes, are quite different from one another, suggesting that different modes of action are operative in each case. To decipher, model and predict the system-level metabolic responses to the treatment of these drugs, we constructed a general GEM model of A2780 cancer cells. We contextualized such reconstructions using extracellular metabolomic and gene expression data and generated reconstructions specific to each gold drug treatment. Such models were able to correctly predict the change in concentration of approximately 70% of the experimentally measured metabolites included in the A2780 reconstruction. In-depth analysis of these responses revealed the occurrence of distinct metabolic responses to each gold drug, suggesting that while there are some common features in cancer cell responses to these gold drugs, each drug induces specific changes in the cellular metabolic network. Ideally, understanding which parts of the metabolism are most affected by the drugs may help to optimize these treatments, for example by suggesting potential (metabolic) adjuvants and/or complementary drugs to be used in combination with the drugs discussed here²⁴. Overall, the integration of metabolomic data with genome-scale metabolic modeling has confirmed the idea that gold compounds can directly or indirectly target multiple metabolic pathways in tumor cells, leading to profound changes in tumor cells and their microenvironment⁴⁸. Together with a recent and comprehensive study from Meeson and Schwartz⁴⁹, this work provides one of the first genome-

wide descriptions of the metabolic reprogramming occurring in ovarian cancer cells, also highlighting the importance of integrating -omics data with computational models to address context-specific issues in medical sciences.

Material and methods

Metal compounds

Au(NHC)Cl and [Au(NHC)₂]PF₆ are two gold(I) carbene complexes featuring a 1-butyl-3-methyl-imidazole-2-ylidene moiety as the NHC ligand, coordinated to the gold center via a direct gold-carbon bond. These compounds differ in their second ligand: a chloride in Au(NHC)Cl or another NHC ligand in [Au(NHC)₂]PF₆; this second ligand influences the lipophilic character of the two gold complexes (Table S2). The synthesis of both gold compounds was carried out according to the procedure reported in the paper of Messori et al.⁵⁰

Sodium aurothiomalate (Merck, cod: 157201) and auranofin (Enzo Life Sciences, Farmingdale, New York), were used. While auranofin is a linear gold(I) complex with triethylphosphine and tetracetylthioglucose ligands, Aurothiomalate is a (1,2-Dicarboxyethylthio)gold disodium salt hydrate with a more intricate structure⁵¹, indeed its oligomerization in solution has been extensively studied using various physical techniques^{52,53}. Auranofin and Au(NHC)Cl exhibit comparable low solubility in aqueous buffer, as evidence by their similar logP value (Table S2). Conversely, AuTM demonstrates a significant solubility in water, in line with its negative logP value (Table S2).

Cell lines and drug treatment experiments

The cytotoxicity of the four gold(I) compounds on A2780 cells was evaluated via the MTT (3-(4,5-dimethylthiazol-2-yl)-2,5-diphenyltetrazolium bromide) assay. The procedure, reported elsewhere, involved determining the half-maximal inhibitory concentration (IC₅₀) values of each compound after a 72-hour exposure of cells to the metal compound.

Samples for metabolomics were prepared using equitoxic amounts of each metal compound for 24 h, i.e. treating cells for 24 h with a concentration of the gold(I) compound equal to the corresponding IC₅₀ value measured at 72 h, following a well-established approach²⁶.

Metabolomics

Untargeted metabolomics analyses on cell lysates and growth media were performed as in previous reports^{18,26,27}, using a Bruker 600 MHz spectrometer (Bruker BioSpin) optimized for metabolomic analysis, operating at 600.13 MHz proton Larmor frequency and equipped with a 5 mm PATXI ¹H-¹³C-¹⁵N and ²H-decoupling probe including a z-axis gradient coil, an automatic tuning-matching (ATM) and an automatic refrigerated sample changer (SampleJet, Bruker BioSpin). The spectra of cell lysate samples were acquired with the Carr-Purcell-Meiboom-Gill (CPMG) sequence; those of the growth media were acquired with a 1D nuclear Overhauser enhancement spectroscopy (NOESY)-presaturation pulse sequence. Spectra processing was performed using TopSpin 3.6 (Bruker Biospin srl).

Metabolomic data analysis

Well-resolved peaks were assigned to metabolites and their intensities used to quantify the metabolite concentrations in the sample. The assignment was performed using the Chenomx software. The relative quantification of the NMR signals was performed using an R script developed in-house; 32 metabolites were quantified both in the cell lysate spectra and in the growing medium spectra (same number but not the same molecules). In the growth media, the metabolites were divided into two different classes, i.e. those that are taken up from the medium (20 metabolites) and those that are released into the medium (12 metabolites).

All the statistical analyses were performed using the “R” software. The nonparametric pairwise Wilcoxon-Mann-Whitney test was used for the determination of the meaningful metabolites; a *p* value < 0.05 was considered statistically significant. The Log₂ fold change (log₂(FC)) was calculated for each metabolite to display how the metabolite levels vary upon the different treatments. FC is calculated as the median of the ratio of the

metabolite concentrations in the spectra of the two paired samples (treated vs. control). For the growth media analysis, in the case of the released molecules, lower/higher concentration levels upon treatment mean a lower/higher release, while for the molecules that are taken up from the growth media, lower levels upon treatment mean a greater consumption of nutrients, i.e. increased uptake, and vice versa for higher levels.

Ovarian cancer genome-scale metabolic reconstruction

The context-specific genome-scale model of epithelial ovarian cancer cells A2780 was created from the most complete genome-scale model of human metabolism RECON3D⁵⁴ which includes 13,543 metabolic reactions involving 4140 metabolites. We constrained the RECON3D model with transcriptomic data of A2780 cell line present in Cancer Cell Line Encyclopedia (dataset: CCLE_expression_full_22Q2 <https://depmap.org/portal/download/all/>). The RNAseq values are inferred using the RSEM tool and are reported after Log₂ transformation, using a pseudo-count of 1, Log₂(TPM + 1)⁵⁵. In order to match the genes present in RNA-seq dataset with the RECON3D gene identifiers, we used the approach present in Weglarz-Tomczak et al.³¹ with MyGene.py tool version 3.1.0. Afterwards, we applied Gene Inactivity Moderated by Metabolism and Expression (GIMME), which uses quantitative gene expression data and one or more metabolic objectives³⁰ to build context-specific models. The algorithm requires a threshold of gene expression value below which genes are declared as inactive. However, this threshold is dataset-dependent and cannot be reliably inferred a priori. For this reason, we used an “elbow strategy” approach to define the most-reliable gene-expression threshold. We measured the number of metabolites, reactions, cancer-related reaction^{32–35}, that were maintained in the context-specific reconstruction for different values of GIMME threshold. The chosen threshold was the value beyond which the ratio between these and their corresponding values in the original Recon3D reconstruction remained constant. These simulations were performed with COBRA Toolbox v3.0⁵⁶ run in Matlab (version R2022b) and the Gurobi solver (version 9).

Context-specific models reconstruction using metabolomic data

Meeson and Schwartz⁴⁹, have recently proposed metabolic reconstructions of subtype-specific ovarian cancer cells. In their work, they used transcriptomic data to build context-specific models and to study how the regulation of specific pathways links to individual phenotypes. Here, we made use of both transcriptomic and metabolomic data to derive treatment-specific metabolic reconstruction of A2780 cell line. More specifically, for each experimental condition described before, we used the absolute concentration of each identified metabolite at *t* = 0 h and *t* = 24 h to compute the overall nutrient uptake by ovarian cancer cells. We divided the absolute concentration for 24 h and we set the corresponding exchange reactions in the model to such positive (nutrients released in the medium) or negative (nutrients uptake from the medium). Preliminary growth simulations were performed using Flux Balance Analysis (FBA) optimizing for the biomass objective function. However, to obtain more reliable flux distributions for each condition (see below) we used FS, thus focusing on the estimated probability distribution for each reaction's flux in the network. The method present in COBRApy OptGpSampler⁵⁷ allowed us to generate 100 samples for each condition with a thinning factor of 100. Then we calculated the mean of reaction flux for each treatment and its respective control.

Both in FBA and FS we calculated the *p*-value, via the Wilcoxon test (*p*-value threshold 0.05), and the fold-change from the reaction flow between treatments and controls with the R fold change function present in the R tool package.

Data availability

The NMR data used as input for this study are available at the NIH Common Fund's National Metabolomics Data Repository (NMDR) Web site, the Metabolomics Workbench, (37) <https://www.metabolomicsworkbench.org> where it has been assigned Study ID ST003416. The data can be accessed directly via its Project <https://doi.org/10.21228/M8C54J>. This work is

supported by NIH grant U2C-DK119886 and OT2-OD030544 grants. The code and files for genome-scale model construction are available here: <https://doi.org/10.5281/zenodo.15262102>.

Received: 11 February 2025; Accepted: 12 May 2025;

Published online: 28 July 2025

References

- Schoutrop, E. et al. Molecular, cellular and systemic aspects of epithelial ovarian cancer and its tumor microenvironment. *Semin. Cancer Biol.* **86**, 207–223 (2022).
- Torre, L. A. et al. Ovarian cancer statistics. 2018. *CA A Cancer J. Clin.* **68**, 284–296 (2018).
- Koppenol, W. H., Bounds, P. L. & Dang, C. V. Otto Warburg's contributions to current concepts of cancer metabolism. *Nat. Rev. Cancer* **11**, 325–337 (2011).
- Jones, N. P. & Schulze, A. Targeting cancer metabolism – aiming at a tumour's sweet-spot. *Drug Discov. Today* **17**, 232–241 (2012).
- Kobayashi, H. Recent advances in understanding the metabolic plasticity of ovarian cancer: A systematic review. *Heliyon* **8**, e11487 (2022).
- Nantasupha, C., Thonusin, C., Charoenkwan, K., Chattipakorn, S. & Chattipakorn, N. Metabolic reprogramming in epithelial ovarian cancer. *Am. J. Transl. Res.* **13**, 9950–9973 (2021).
- Colombo, N. et al. ESMO–ESGO consensus conference recommendations on ovarian cancer: pathology and molecular biology, early and advanced stages, borderline tumours and recurrent disease. *Ann. Oncol.* **30**, 672–705 (2019).
- Adhikari, S. et al. A review on metal complexes and its anti-cancer activities: Recent updates from in vivo studies. *Biomed. Pharmacother.* **171**, 116211 (2024).
- Moreno-Alcántar, G., Picchetti, P. & Casini, A. Gold complexes in anticancer therapy: From new design principles to particle-based delivery systems. *Angew. Chem. Int. Ed.* **62**, e202218000 (2023).
- Nobili, S. et al. Gold compounds as anticancer agents: Chemistry, cellular pharmacology, and preclinical studies. *Med. Res. Rev.* **30**, 550–580 (2010).
- Abbasi, M., Yaqoob, M., Haque, R. A. & Iqbal, M. A. Potential of gold candidates against human colon. *Cancer MRM* **21**, 69–78 (2021).
- Rigobello, M. P., Scutari, G., Boscolo, R. & Bindoli, A. Induction of mitochondrial permeability transition by auranofin, a Gold(I)-phosphine derivative. *Br. J. Pharmacol.* **136**, 1162–1168 (2002).
- Messori, L. et al. Molecular recognition of metal complexes by DNA: A comparative study of the interactions of the parent complexes [PtCl(TERPY)]Cl and [AuCl(TERPY)]Cl₂ with double stranded DNA. *Bioinorg. Chem. Appl.* **3**, 239–253 (2005).
- Liu, W. & Gust, R. Metal N-heterocyclic carbene complexes as potential antitumor metallodrugs. *Chem. Soc. Rev.* **42**, 755–773 (2013).
- Vitali, V., Massai, L. & Messori, L. Strategies for the design of analogs of auranofin endowed with anticancer potential. *Expert Opin. Drug Discov.* **19**, 855–867 (2024).
- Magherini, F. et al. Antiproliferative effects of two gold(I)-N-heterocyclic carbene complexes in A2780 human ovarian cancer cells: a comparative proteomic study. *Oncotarget* **9**, 28042–28068 (2018).
- Magherini, F. et al. Exploring the biochemical mechanisms of cytotoxic gold compounds: a proteomic study. *J. Biol. Inorg. Chem.* **15**, 573–582 (2010).
- Cosottini, L. et al. Unlocking the power of human ferritin: Enhanced drug delivery of aurothiomalate in A2780 ovarian cancer cells. *Angew. Chem. Int. Ed.* **63**, e202410791 (2024).
- Massai, L. et al. The effects of two gold-N-heterocyclic carbene (NHC) complexes in ovarian cancer cells: a redox proteomic study. *Cancer Chemother. Pharm.* **89**, 809–823 (2022).
- Gamberi, T., Pratesi, A., Messori, L. & Massai, L. Proteomics as a tool to disclose the cellular and molecular mechanisms of selected anticancer gold compounds. *Coord. Chem. Rev.* **438**, 213905 (2021).
- Ghini, V. et al. Novel NMR-based approach to reveal the 'Metabolic Fingerprint' of cytotoxic gold drugs in cancer cells. *J. Proteome Res.* **24**, 813–823 (2025).
- Chiappetta, G. et al. Redox proteome analysis of auranofin exposed ovarian cancer cells (A2780). *Redox Biol.* **52**, 102294 (2022).
- Opdam, S. et al. A Systematic Evaluation of Methods for Tailoring Genome-Scale Metabolic Models. *Cell Syst.* **4**, 318–329.e6 (2017).
- Bintener, T. et al. Metabolic modelling-based in silico drug target prediction identifies six novel repurposable drugs for melanoma. *Cell Death Dis.* **14**, 468 (2023).
- Pacheco, M. P. et al. Identifying and targeting cancer-specific metabolism with network-based drug target prediction. *eBioMedicine* **43**, 98–106 (2019).
- Ghini, V. Cell Metabolomics to Guide the Design of Metal-Based Compounds. *Inorganics* **12**, 168 (2024).
- Ghini, V. et al. NMR reveals the metabolic changes induced by auranofin in A2780 cancer cells: evidence for glutathione dysregulation. *Dalton Trans.* **50**, 6349–6355 (2021).
- Ghini, V. et al. The effects of two cytotoxic gold(I) carbene compounds on the metabolism of A2780 ovarian cancer cells: Mechanistic inferences through NMR analysis. *RSC Adv.* **13**, 21629–21632 (2023).
- Ghandi, M. et al. Next-generation characterization of the cancer cell line encyclopedia. *Nature* **569**, 503–508 (2019).
- Becker, S. A. & Palsson, B. O. Context-specific metabolic networks are consistent with experiments. *PLoS Comput. Biol.* **4**, e1000082 (2008).
- Weglarz-Tomczak, E., Mondeel, T. D. G. A., Piebes, D. G. E. & Westerhoff, H. V. Simultaneous integration of gene expression and nutrient availability for studying the metabolism of hepatocellular carcinoma cell lines. *Biomolecules* **11**, 490 (2021).
- Nilsson, A. & Nielsen, J. Genome scale metabolic modeling of cancer. *Metab. Eng.* **43**, 103–112 (2017).
- Zielinski, D. C. et al. Systems biology analysis of drivers underlying hallmarks of cancer cell metabolism. *Sci. Rep.* **7**, 41241 (2017).
- Gatto, F., Ferreira, R. & Nielsen, J. Pan-cancer analysis of the metabolic reaction network. *Metab. Eng.* **57**, 51–62 (2020).
- Yizhak, K., Chaneton, B., Gottlieb, E. & Ruppin, E. Modeling cancer metabolism on a genome scale. *Mol. Syst. Biol.* **11**, 817 (2015).
- Madeira, J. M., Gibson, D. L., Kean, W. F. & Klegeris, A. The biological activity of auranofin: implications for novel treatment of diseases. *Inflammopharmacol.* **20**, 297–306 (2012).
- Koundouros, N. & Poulogiannis, G. Reprogramming of fatty acid metabolism in cancer. *Br. J. Cancer* **122**, 4–22 (2020).
- Farahzadi, R. et al. Clinical significance of carnitine in the treatment of cancer: from traffic to the regulation. *Oxid. Med. Cell. Longev.* **2023**, 1–15 (2023).
- Seko, A. et al. N-Acetylglucosamine 6-O-sulfotransferase-2 as a tumor marker for uterine cervical and corpus cancer. *Glycoconj. J.* **26**, 1065–1073 (2009).
- Al-Khallaif, H. Isocitrate dehydrogenases in physiology and cancer: biochemical and molecular insight. *Cell Biosci.* **7**, 37 (2017).
- Liu, S., Cadoux-Hudson, T. & Schofield, C. J. Isocitrate dehydrogenase variants in cancer — Cellular consequences and therapeutic opportunities. *Curr. Opin. Chem. Biol.* **57**, 122–134 (2020).
- Byrne, F. L. et al. Phenotypic screen for oxygen consumption rate identifies an anti-cancer naphthoquinone that induces mitochondrial oxidative stress. *Redox Biol.* **28**, 101374 (2020).
- Shan, M., Yang, D., Dou, H. & Zhang, L. Fucosylation in cancer biology and its clinical applications. in *Progress in Molecular Biology and Translational Science* 162 93–119 (Elsevier, 2019).

44. Pavlova, N. N. et al. As extracellular glutamine levels decline, asparagine becomes an essential amino acid. *Cell Metab.* **27**, 428–438.e5 (2018).
45. Zhang, J. et al. Asparagine plays a critical role in regulating cellular adaptation to glutamine depletion. *Mol. Cell* **56**, 205–218 (2014).
46. Kudelka, M. R., Ju, T., Heimbürg-Molinari, J. & Cummings, R. D. Simple Sugars to Complex Disease—Mucin-Type O-Glycans in Cancer. in *Advances in Cancer Research* 126 53–135 (Elsevier, 2015).
47. Moseley, H. N., Lane, A. N., Belshoff, A. C., Higashi, R. M. & Fan, T. W. A novel deconvolution method for modeling UDP-N-acetyl-D-glucosamine biosynthetic pathways based on 13 C mass isotopologue profiles under non-steady-state conditions. *BMC Biol.* **9**, 37 (2011).
48. Kou, L., Wei, S. & Kou, P. Current progress and perspectives on using gold compounds for the modulation of tumor cell metabolism. *Front Chem.* **9**, 733463 (2021).
49. Meeson, K. E. & Schwartz, J.-M. Constraint-based modelling predicts metabolic signatures of low and high-grade serous ovarian cancer. *npj Syst. Biol. Appl* **10**, 96 (2024).
50. Messori, L. et al. Chemistry and biology of two novel gold(I) carbene complexes as prospective anticancer agents. *Inorg. Chem.* **53**, 2396–2403 (2014).
51. Hill, D. T. et al. Gold-197 Moessbauer studies of some gold(I) thiolates and their phosphine complexes including certain antiarthritic gold drugs. *Inorg. Chem.* **22**, 2936–2942 (1983).
52. Bau, R. Crystal structure of the antiarthritic drug gold thiomalate (myochrysine): A double-helical geometry in the solid state. *J. Am. Chem. Soc.* **120**, 9380–9381 (1998).
53. Tieckink, E. R. T. Gold derivatives for the treatment of cancer. *Crit. Rev. Oncol. /Hematol.* **42**, 225–248 (2002).
54. Brunk, E. et al. Recon3D enables a three-dimensional view of gene variation in human metabolism. *Nat. Biotechnol.* **36**, 272–281 (2018).
55. Barretina, J. et al. The cancer cell line encyclopedia enables predictive modelling of anticancer drug sensitivity. *Nature* **483**, 603–607 (2012).
56. Heirendt, L. et al. Creation and analysis of biochemical constraint-based models using the COBRA Toolbox v.3.0. *Nat. Protoc.* **14**, 639–702 (2019).
57. Megchelenbrink, W., Huynen, M. & Marchiori, E. optGpSampler: An improved tool for uniformly sampling the solution-space of genome-scale metabolic networks. *PLoS ONE* **9**, e86587 (2014).

Acknowledgements

L.M. gratefully acknowledges funding by AIRC, IG 2021 ID 26169 “Multi-Omics approach to establish the molecular mechanisms of Anticancer Gold Compounds in the Systems Biology Era”. P.T. and V.G. acknowledge the support and the use of resources of Instruct-ERIC, a Landmark ESFRI project, and specifically the CERM/CIRMMP Italy Center, and the project Potentiating the Italian Capacity for Structural Biology Services in Instruct-ERIC, Acronym “ITACA.SB” (Project no. IR0000009) within the call MUR

3264/2021 PNRR M4/C2/L3.1.1, funded by the European Union – NextGenerationEU. This work has received funding from the Italian Ministry of Education and Research (MUR), through Department di Eccellenza 2023–2027 (DICUS 2.0) to the Department of Chemistry “Ugo Schiff” of the University of Florence.

Author contributions

W.V. Writing—review & editing, Data analysis, Validation, Conceptualization. V.G. Writing—review & editing, Data analysis. P.T. Writing—review & editing, Conceptualization. L. Massai. Writing—review & editing, Conceptualization. L. Messori. Writing—review & editing, Conceptualization. Funding acquisition. M.F. Writing—review & editing, Writing—original draft, Methodology, Investigation.

Competing interests

The authors declare no competing interests.

Additional information

Supplementary information The online version contains supplementary material available at <https://doi.org/10.1038/s41540-025-00535-9>.

Correspondence and requests for materials should be addressed to Luigi Messori or Marco Fondi.

Reprints and permissions information is available at <http://www.nature.com/reprints>

Publisher’s note Springer Nature remains neutral with regard to jurisdictional claims in published maps and institutional affiliations.

Open Access This article is licensed under a Creative Commons Attribution-NonCommercial-NoDerivatives 4.0 International License, which permits any non-commercial use, sharing, distribution and reproduction in any medium or format, as long as you give appropriate credit to the original author(s) and the source, provide a link to the Creative Commons licence, and indicate if you modified the licensed material. You do not have permission under this licence to share adapted material derived from this article or parts of it. The images or other third party material in this article are included in the article’s Creative Commons licence, unless indicated otherwise in a credit line to the material. If material is not included in the article’s Creative Commons licence and your intended use is not permitted by statutory regulation or exceeds the permitted use, you will need to obtain permission directly from the copyright holder. To view a copy of this licence, visit <http://creativecommons.org/licenses/by-nc-nd/4.0/>.

© The Author(s) 2025